Defect Microstructure Evolution in an Immiscible Composite Cu43%Cr Alloy after High-Pressure Torsion and Annealing using Positron Annihilation Spectroscopy

I. Bibimoune[a], E. Hirschmann[b], M. O. Liedke[b], A. Wagner[b], M. Kawasaki[c], T. Baudin[d], I. Mkinsi[d], K. Abib[a], Y. Huang[e,f], T. G. Langdon[f], D. Bradai[a]

[a] Laboratory of Materials Physics, Faculty of Physics, University of Sciences and Technology Houari Boumediene, BP 32 El Alia, Bab-Ezzouar, 16111, Algiers, Algeria.
[b] Institute of Radiation Physics, Helmholtz-Zentrum Dresden – Rossendorf, Bautzner Landstr. 400, 01328 Dresden, Germany
[c] School of Mechanical Industrial and Manufacturing Engineering, Oregon State University Corvallis, OR 97331, USA
[d] Université Paris-Saclay, CNRS, Institut de Chimie Moléculaire et des Matériaux d'Orsay, 91405 Orsay, France
[e] Department of Design and Engineering, Faculty of Science and Technology, Bournemouth University, Poole, Dorset BH12 5BB, UK
[f] Materials Research Group, Department of Mechanical Engineering, University of Southampton, Southampton SO17 1BJ, UK
[*]Corresponding author: imenebibmoune2017@gmail.com

Abstract

The microstructure of a Cu43%Cr alloy after high-pressure torsion (HPT) processing and annealing for 1 hour was analyzed using Doppler broadening – variable energy PAS (DB-VEPAS) and conventional positron annihilation lifetime spectroscopy (cPALS). DB-VEPAS analysis of the near-surface defects reveals the existence of a nanosized oxide layer whose thickness increases from 43 nm to 103 nm with temperature (210°C-850 °C) while the diffusion length is unaffected around 20 nm. cPALS analysis revealed two lifetime components of the bulk defects, namely the components related to either vacancies or dislocations, for the as-received material with annealing at 925°C. After HPT processing, the alloy showed two components which correspond to positrons trapped and annihilated at dislocations (lifetime~ 160 ps) in Cu and Cr and at clusters of vacancies (about 13-10 vacancies). The intensity of the first component decreases with increasing annealing temperatures from 210 to 850 °C, thereby implying a partial annihilation of dislocations due to microstructure recovery. The variation of the second component depends on the variation of vacancy cluster size (from about 13 and 10 to about 4 vacancies) resulting from different annealing temperatures. Additionally, Vickers microhardness measurements show that the alloy is substantially hardened after processing by HPT for N = 20 turns. After annealing for 1 hour at 210, 550 and 850°C, the HPT-processed alloy after 5 turns demonstrated a gradual softening by microstructural recovery. Annealing-induced hardening is observed after HPT for 20 turns followed by heating up to 550°C while softening is observed after annealing at 850°C.

Keywords: Cu-Cr; defects; immiscible alloys; high-pressure torsion; positron annihilation spectroscopy.

1. Introduction

Immiscible metallic alloy systems, such as Cu-X systems with alloy elements having different melting temperatures, have motivated considerable interest over the last decades owing to their desired mechanical, electrical and physical properties [1]. Within the immiscible alloys, Cu-X (X = Cr, W, Fe, Ta, Mo etc.) pseudo-alloys are often prepared by mechanical alloying. Cu‑Cr pseudo-alloys are characterized by the existence of two classes. The first class concerns the copper alloys containing 1-10 wt.% addition of chromium [2, 3]. Due to the very low solubility of Cr of 1 at.% in solid Cu, the alloys dissolve Cr in an oversaturated solid solution or contain it in metal clusters. The second class Cu‑Cr is outlined by composites containing essentially equal mass fractions of Cu and Cr [4, 5]. For this second class, the immiscible Cu- and Cr-based phases form two phase microstructure morphology.

The motivation for the development of immiscible Cu-Cr alloy is twofold : (i) Industrial applications such as contact wires and cables for railways [6], lead frames in integrated circuits [7] and electric contacts in high voltage electrical circuits [4, 8], and (ii) functional properties that can be further improved. Indeed, the Cu-Cr alloys are promising in applications that require an optimum combination of mechanical strength and electrical conductivity as well as excellent oxidation and corrosion resistance [9]. Contrarily to pure Cu, after standard thermal treatments these alloys show an ultimate tensile strength of more than 450 MPa and 75 to 85 % IACS and thermal stability up to a temperature of 450°C [9, 10]. For academic consideration, Cu-Cr alloy represents one of the model nanostructured systems when considering the microstructure-properties correlations as well as the thermal stability [11, 12]. Indeed, as stated by Kormout et al. [13] composites of immiscible alloys are very attractive owing to their higher structural and thermal stability than those of single-phase alloys. A positive Gibbs free energy change for forming a solid-solution alloy in the equilibrium state is characteristic of this binary immiscible system in the solid state [11]. Nevertheless, many authors have evidenced the formation of

supersaturated solid solution during ball milling (BM) [14, 15] or after severe plastic deformation by high-pressure torsion [12]. Moreover, these non-equilibrium processing techniques have been shown to ensure tunable ultrafine nano-grained microstructures [16].

The immiscibility of this alloy system is determined by the maximum solubility of Cu in body-centered cubic (bcc) Cr of less than 0.2 at.% and Cr in face-centered cubic (fcc) Cu of 0.89 at% at 1350 K. No intermetallic phase is found in the available phase diagram of the system [17].

To date, the mechanical properties, microstructure, nanostructure, phase transformation, and sub-nanometer scale compositions have been thoroughly analyzed in Cu43%Cr alloy after high-pressure torsion (HPT) using a series of techniques including atom probe tomography (APT), X-ray diffraction (XRD), energy-dispersive synchrotron diffraction (EDXS), high resolution and scanning electron microscopy (HRTEM, STEM) [1, 12, 18, 19]. Besides the significant microstructural refinement leading to the strengthening of the material, HPT processing introduces shear-induced intermixing of normally an immiscible binary system into a non-equilibrium condition. For instance, supersaturated solutions (SSSSs) of Cu in the Cr phase up to 15 at.% (equivalent to 17.7 wt.%) were formed while missing the formation of SSSSs of Cr in the Cu phase [1].

It is well known that SPD introduces a large number of crystal defects (vacancies, dislocations, stacking faults, twins, grain boundaries, etc.) in the material, and the defect densities increase by increasing the total amount of imposed strain. In practice, the lattice parameter can be affected by deformation-induced defects such as vacancies [20]. A recent report by Shao et al. [19] quantitatively estimated the densities of different types of defects including stacking faults, deformation twins, and edge dislocations in a nanostructured 57 wt%Cu-43 wt%Cr alloy after HPT for 5 and 25 turns. Apart from this report, the evolution of defects, mainly dislocations and vacancies, has not been reported for an immiscible composite Cu-Cr alloy after grain refinement through SPD and subsequent heating. Accordingly, this work aims to evaluate the

defect microstructure in a Cu-Cr alloy after HPT processing and annealing using two different Positron annihilation spectroscopies (PAS). Firstly, Doppler broadening – variable energy PAS (DB-VEPAS [21]) for the identification of the in-depth distribution of defects, and secondly PA-lifetime spectroscopy (PALS) for the identification of the defect nature and density in bulk [21]. Additionally, microhardness measurements to support the discussion on the processing-microstructure-mechanical property relationship. The results obtained are compared and discussed based on the literature and recently published X-ray diffraction data [22].

2 Experimental materials and procedures

The present study was carried out on a Cu43%Cr (wt.%) (PLANSEE, Reutte, Austria) immiscible commercial alloy. Samples in the form of discs (10 mm diameter and 1 mm thickness) were cut using an electrical discharge machine. The samples were then subjected to HPT for 5 and 20 turns, under a pressure of 6 GPa and a rotational speed of 1 rpm. After HPT deformation, subsequent annealing was performed at 210, 550 and 850°C for one hour under an Argon environment.

Positron annihilation spectroscopy (PAS) measurements were carried out at the Institute for Radiation Physics at Helmholtz-Zentrum Dresden − Rossendorf (HZDR). The SPONSOR (Slow POsitroN System Of Rossendorf) [21] device is used for DB-VEPAS (Doppler broadening variable energy PAS), enabling materials to be studied in depth with atomic sensitivity. The positrons were produced by ß$^{+}$ decays of a ^{22}Na radioisotope. A well-annealed tungsten foil served as moderator. The positron beam produced is accelerated to energies typically ranging from 0.03 to 35 keV. The positrons are magnetically guided and introduced into the sample at depths of up to a few micrometers. Implantation energy and material density determine the depth of implantation. During implantation, the positrons reduce their energy by inelastic scattering (thermalization) in a few picoseconds (~10 ps) and diffuse through the

lattice until they meet and annihilate with an electron, either directly with free electrons or after trapping in vacancy-like defects and interfaces. Annihilation of the electron-positron pairs results in the emission of two anti-collinear gamma photons of ~511 keV, which is measured with a high purity Ge-detector with a resolution $f_R = 1.09 \pm 0.01$ keV at 511 keV. Thermalized positrons have a significantly lower momentum than electrons, resulting in a line broadening of 511 keV. This line expansion is mainly due to the momentum of electrons.

The conventional positron annihilation lifetime spectroscopy (cPALS) technique, unlike DB-VEPAS, allows the extraction of bulk property details of the whole specimen. cPALS measurements were conducted on Cu43Cr samples at HZDR, Germany using 4CrBr3 scintillator detectors [50.8 mm diameter (=2 inches) and 25.4 mm length (=1 inch)] coupled to Hamamatsu R13089 PMTs, using a SPDevices ADQ14-DC-2X digitizer with 14 bit vertical resolution and 2GS/s horizontal resolution [23] and an instrument resolution function down to about 240 ps. The resolution function required for spectrum analysis uses two Gaussian functions with distinct intensities and appropriate relative shift. All spectra contained at least 1×10^7 counts. Typical lifetime spectrum N(t) is described by:

$$N(t) = \Sigma\ (1/\tau_i)\ I_i \exp(-t/\tau_i) \qquad (1)$$

where τ_i and I_i are the positron lifetime and intensity of the i-th component, respectively ($\Sigma Ii=1$). All the spectra were deconvoluted using a non-linear least-squares fitting method using the fitting software package PALSfit [24] into 4 discrete lifetime components, which directly evidence the different defect states (τ_1 and τ_2). The remaining 2 components τ_3 = 382 ps and τ_4 = 2700 ps were fixed since they belong to the source correction. The corresponding relative intensities reflect a large extent concentration of each defect type (size) as long as the size of compared defects is in a similar range. The relative intensity I_3 (of τ_3) was fixed at 13% and the rest of them were calculated as free parameters. In order to obtain a well-founded determination

of the resolution function and source correction, various reference materials were investigated. These have the property that only one lifetime component is measured in addition to the source components. Consequently, for all reference materials (Al, In, Sn, Ta), both the resolution function and the source correction were determined as constants.

Vickers microhardness (Hv) values were collected with a load of 0.98 N and a dwell time of 10 s in a Zwick 3212 microhardness apparatus. The microhardness was taken near the surface of the shear plane at ~0.3 mm from the disk center across the radius of each disc, where the microhardness value was averaged in four separate measurements.

3 Results and Discussion

3.1 Near surface defects analysis

DB-VEPAS results are often presented in terms of the S and W parameters as a function of energy (E_p). These parameters are defined as the fraction of positron annihilations with free and valence electrons (low-momentum electrons) and with core electrons (high-momentum electrons), respectively [25]. The S and W parameters are determined by the area under the central portion of the annihilation line (511±0.93 keV) and in the wing regions of the line (508.56±0.35 keV and 513.44±0.35 keV) divided by the total area under the line. A Makhovian function was considered in order to calculate the mean positron implantation depth, *Z*. In its simple expression, it is given by [26] :

$$z = \frac{3.6E_p^n}{\rho} \quad (2)$$

where *Ep* is the implantation energy in keV. The n parameter was taken as n = 1.62 and the density, ρ, of the Cu43%Cr composite was taken from the tabulated data of ρ = 7.62 g/cm^3 measured according to the Archimedean principle [27].

Figure 1 shows the values of the S and W parameters at upper and lower rows, respectively, as a function of *Ep* and *Z* at lower and upper horizontal axes, respectively, for the Cu43%Cr alloy in a) as-received (N = 0 turn), and after HPT processing for b) N = 5 turns and c) N = 20 turns followed by annealing. In general, the value of the S parameter decreases with increasing energy and levels off when the positron implantation energy reaches a value equal to 15 keV for almost all samples. Moreover, the S parameter decreases after HPT processing followed by annealing at any annealing temperature applied relative to the non-deformed state. This decrease as a function of the number of revolutions is believed to be due to the annihilation of vacancies existing close to the surface of the sample in sinks at grain boundaries and the surface [28].

Cizek et al. [28] explained that a part of the deformation-induced vacancies disappear by diffusion to sink at grain boundaries and the surface, and the concentration of vacancies surviving in the HPT-deformed sample represents 40-50% of the net concentration of the deformation-induced vacancies. The fraction of vacancies lost by diffusion to sinks increases at a higher number of turns, N, since sink density increases with grain refinement. After annealing at 210, 550 and 850°C, there is a tendency to increase the S parameter, while it is limited in the sample after N = 5. This increasing value of the S parameter is due to an increase in the number of open-volume defects in the sample surfaces most likely as a result of i): oxidation processes and/or ii) thermal vacancies generated within solids at high temperatures are somehow stabilized, e.g., due to interactions with different vacancies. The lower row in Figure 1 shows that the S parameter is negatively correlated with the W parameter. As soon as an open volume defect traps a positron, it localizes its wave function and therefore results in a reduction of its overlap with high-momentum core electrons and the loss of the broadening of the annihilation photopeak. Let us remind that a photopeak is a full energy peak that occurs when a gamma ray transfers its full energy to the sensitive material (scintillation crystal). As a

consequence, the S parameter increases [28] and W decreases, where such opposite behaviors with increasing implementation energy are apparent in Figure 1.

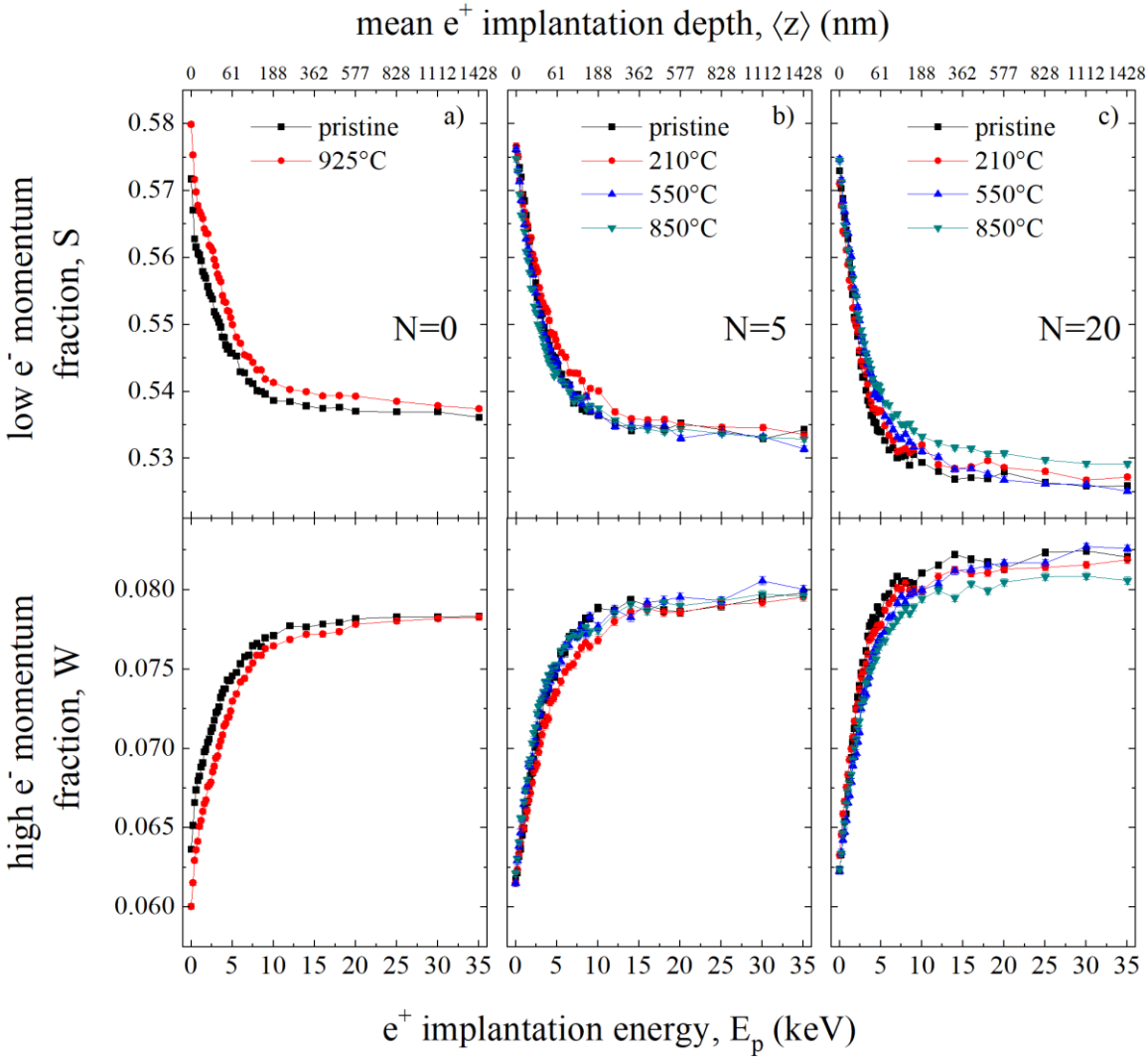

Figure 1: Annihilation line parameter S (low electron momentum fraction) and W (high electron momentum fraction) as a function of positron implantation energy E_p and mean positron implantation depth <z>, (a) (N=0 and annealing at 925°C), (b) (N=5 and annealing at 210°C, 550°C, 850°C) and (c) (N=20 and annealing at 210°C, 550°C, 850°C).

The S-W curve is used to determine the change in defect types, and it is displayed in Figure 2 for the Cu43%Cr alloy after HPT for (a) N = 0 turn, (b) N = 5 turns and (c) N = 20 turns followed by heating at different temperatures. Indeed, any slope change of the S-W curve indicates a change in the nature and type of defects. As shown in Figure 2, the slopes of the

curves did not change with different thermo-mechanical processes which means that the type of defects did not vary.

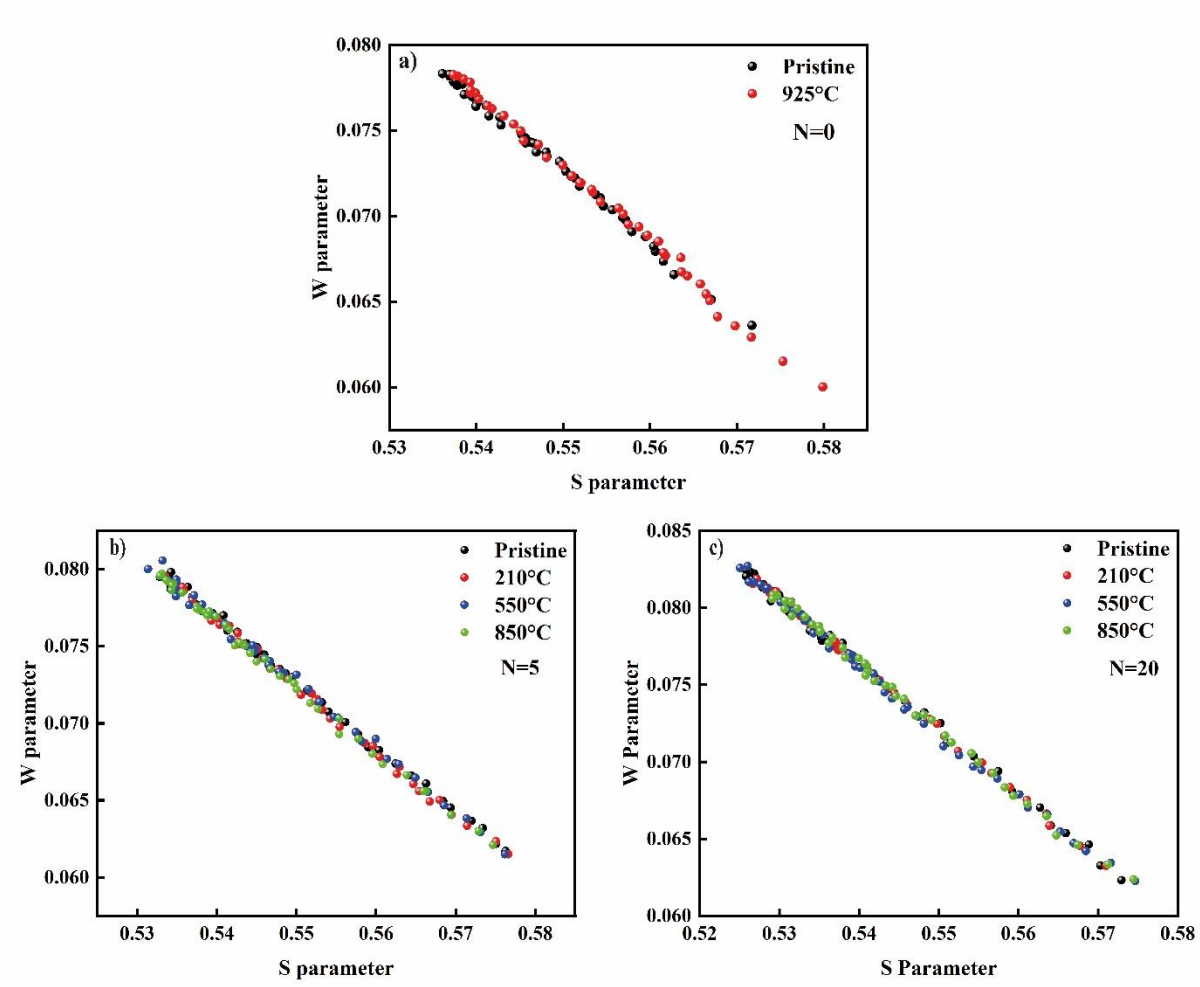

Figure 2: Plots of W parameter versus S parameter. (a) (N=0 and annealing at 925°C), (b) (N=5 and annealing at 210°C, 550°C, 850°C) and (c) (N=20 and annealing at 210°C, 550°C, 850°C).

The S-parameter depth profiles were then analyzed using the VEPFIT code developed by van Veen et al. [29]. This code numerically solves the positron diffusion equation and gives the characteristic parameters, i.e. the positron effective diffusion lengths in the various layers of the system. After accurate fits of the S(*Ep*) curves, the thickness and effective positron diffusion length L+ for each layer can be deduced. While running VEPFIT software, the material was considered as containing two layers of the surface oxide L_1+ and the bulk material L_2+. These effective positron diffusion lengths and the calculated oxide layer thickness d are summarized

in Table 1 for all tested sample conditions, where the number after N and T provides the number of HPT turns and applied annealing temperature in °C with time in an hour, respectively.

Table 1. Calculated thickness of the oxide layer, d, and positron diffusion lengths of the oxide layer L_1+ and bulk L_2+ in Cu43%Cr alloy after HPT and annealing. The values without errors were fitted as fixed accounting for the lowest chi-square. All length values are in nm.

	N0-T25	**N0-T925-6h**	**N5-T25**	**N5-T210-1h**	**N5-T550-1h**	**N5-T850-1h**	**N20-T25**	**N20-T210-1h**	**N20-T550-1h**	**N20-T850-1h**
d (nm)	30±24	53±13	47±42	68	48	73	60	82±44	94	103±72
L_1+ (nm)	23±3	23±2	18±1	26±1	17±1	16±1	20±1	21±1	23±1	21±1
L_2+ (nm)	56±5	48±10	49±8	102±13	76±9	150±45	44±19	83±27	184±33	149±69

From Table 1, it can be seen that the oxide layer thickness d ≈ 30 nm in N0-T25 increases as the number of revolutions increases to ~47 nm and ~ 60 nm after 5 and 20 HPT turns, respectively. It also increases continuously after thermal annealing at different temperatures, such as up to 103 nm after 20 HPT turns followed by annealing at 850°C. With increasing annealing temperature, the oxide layer becomes thicker and contains more defects whose overall diffusion length is small. It can explain the increase in the S parameter when the HPT-processed samples are annealed as shown in Figure 1. The diffusion length in the sub-surface layer L_1+ is almost constant, ranging from 16 to 23 nm. Furthermore, increasing the annealing temperature extended the positron bulk diffusion length, i.e. reaching L_2+ ≈ 150 nm at 850°C in the N = 20 turns sample, which is caused by recovery of the microstructure and accompanying dislocation annihilation that will be discussed in detail in the next section. For comparison purposes, it is reasonable to note that the scattering length obtained from a reference sample of a fully annealed Cr (1000 °C, 10 h, at $<10^{-8}$ mbar) (without oxide) is L+ ~ 130 nm [30] and the diffusion length in non-deformed pure copper is ~146 nm [31]. Based on these

findings, one can state that the annealing increased the oxide thickness and caused the annihilation of defects in the bulk.

3.2 Bulk defects analysis

The cPALS measurements revealed two separate lifetime components in the measured spectra of the Cu43%Cr alloy at all different thermomechanical processing conditions. Figure 3 presents the evolution of positron lifetime (cPALS) components τ_1 and τ_2 and their relative intensities I_1 and I_2 in left and right columns, respectively, for the Cu43%Cr alloy at the different thermomechanical conditions (number of HPT turns and thermal annealing temperatures). The horizontal dashed lines represent different lifetimes of bulk, $\tau_B^{Cu,Cr}$ [32,33], one vacancy $V_1^{Cu,Cr}$ [34],[35], and clusters of 4 and 13 vacancies, $V_4^{Cu,Cr}$ and $V_{13}^{Cu,Cr}$ [33,36], respectively, in pure Cu and Cr elements. Details about lifetime of, $V_4^{Cu,Cr}$ and $V_{13}^{Cu,Cr}$ are presented later in the text.

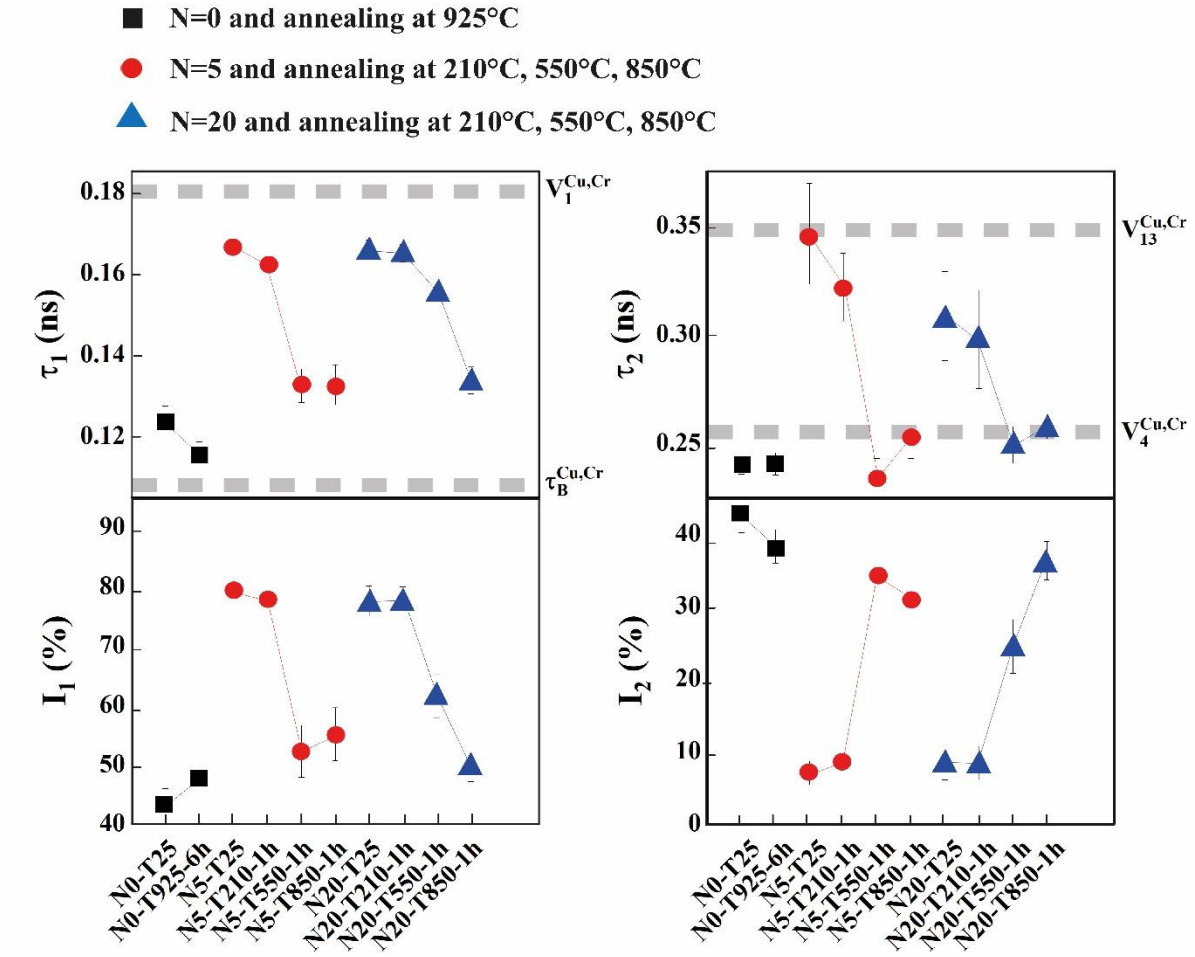

Figure 3: Positron lifetime components τ_1 and τ_2 and their relative intensities I_1 and I_2, respectively, for pristine and HPT-processed samples and subsequent annealing. The horizontal dashed lines represent different lifetimes of bulk, $\tau_B^{Cu,Cr}$, one vacancy $V_1^{Cu,Cr}$ and clusters of 4 and 13 vacancies, $V_4^{Cu,Cr}$ and $V_{13}^{Cu,Cr}$, respectively, in pure Cu and Cr elements.

In both N0-T25 (as-received) and N0-T925-6h (as received + annealed at 925°C for 6 h) samples, the first component with τ_1 ~ 110-120 ps is in the range of positron lifetimes in bulk Cu and Cr [32, 33, 37, 38]. The second component with τ_2 ~ 240 ps represents a contribution from positrons trapped in clusters of about 4 vacancies [36, 33]. The deformed samples without heat treatment (N5-T25, N20-T25) demonstrated the value of τ_1 ~ 166 ps for both cases. It corresponds well with tabulated values in the literature for positrons trapped and annihilated at dislocations in Cu and Cr, see Table 2. The value of τ_2 is ~346 and ~308 ps for N5-T25 and N20-T25, respectively. Thus, the corresponding relative intensities for the two separate lifetime components are I_1 ~78% and I_2 ~8 % for N5-T25 and N20-T25, respectively. These two lifetime components represent the annihilation of the positron at clusters of about 13 and 8 vacancies, respectively.

The positron lifetime spectra were also well decomposed into two major positron lifetime components after thermal annealing of the HPT-processed Cu43%Cr alloy. The first component τ_1 and its intensity I_1 decrease with increasing annealing temperatures and reach values ~133 ps and ~50-55%, respectively, after annealing for 1 h at 850°C, where τ_1 is slightly higher than the lifetime of free positrons $\tau_B^{Cu,Cr}$. This decrease means that there is a partial (not total) annihilation of dislocation and recovery of the severely deformed microstructure. The present results regarding to the first component agree with the earlier reported study by Hakatemaya et al. [32], who analyzed the positron annihilation behavior in a Cu–Cr–Zr alloy after several different aging treatments creating precipitations. They stated that the positron lifetime spectra of the alloy after the heat treatments were well described by a single lifetime component; these

lifetimes were in between the positron lifetime of bulk Cu of 110 ps [39] and monovacancies in pure Cu of 173 ps [39]. Accordingly, the observed positron lifetimes in the present study are expected to be averages of the positron lifetimes resulting in the bulk Cu and vacancy-like defects (including dislocations) which are induced at the interfaces between the Cr-rich precipitates and the Cu matrix.

With annealing, the values of τ_2 for the HPT-deformed Cu43Cr samples decrease from 346 ps in N5-T25 and 308 ps in N20-T25 to close to ~250 ps in both. These lowered values are similar to the non-deformed material of N0-T25 and N0-T925-6h. Moreover, the corresponding intensity increases with thermal processes. The variation of τ_2 is attributed to the variation in vacancy cluster size due to annealing, which means that the size of the vacancy cluster decreases from about 13 in N5-T25 and about 10 in N20-T25 to such as ~ about 4 in both after annealing of N5-T850-1h and N20-T850-1h. Therefore, annealing at 850°C caused a noticeable formation of vacancy clusters while annealing at 210°C for 1h provided a comparably faint effect.

A list of the reported data of the positron lifetimes is summarized in Table 2. It reveals that the positron bulk life time for Cu and Cr varies from 108 to 120 ps [32 , 33 , 37, 38, 40] while for a single vacancy it is around 180 ps in Cu [34, 35] and 184-188 ps in Cr [38, 30]. For both elements, the lifetime in dislocations is around 160–166 ps [30 ,34]. Positron lifetimes for the alkali metals and 4th period elements including both Cu and Cr as well as some selected oxides have been computed using the improved generalized gradient approximation by Kuriplach et al. [40]. The report validated the computed positron lifetimes by demonstrating the similarity with the experimental ones. As listed in Table 2, the present experimental values of the positron bulk lifetimes for Cu and Cr elements agree with the reported value. Other reports utilizing a positron-lifetime spectroscopy approach have discussed two types of lattice defects in ultrafine-grained (UFG) Cu prepared by HPT [34, 41]. One is dislocations in distorted regions along grain boundaries and the other is microvoids consisting of clusters of 3 to 5 vacancies inside

grains. The present results shown in Figure 3 imply the vacancy clusters generated by HPT processing.

The agglomeration of deformation-induced vacancies leading to the vacancy cluster is influenced by the mobility of vacancies [28]. The estimation of the average size of clustered vacancies is available through the theoretical calculation of positron lifetimes with increasing numbers of vacancies in Cu and Cr as shown in Figure 4. A correlation between the vacancy cluster size and positron lifetime has been established for both Cu and Cr [36, 33], where the positron lifetime calculations were performed by standard density functional theory methods. Figure 4 shows the calculated positron lifetime for the number of vacancies presenting the size of vacancy clusters for Cu and Cr. For both Cu and Cr elements, the positron lifetime increases with the size of the vacancy cluster. Cizek et al. [36] have reported that the size distribution of vacancy clusters in HPT-deformed metals is not correlated to their crystal structure but rather related to the activation energy for vacancy migration. The vacancy migration energies of Cu and Cr are close, such as E_{Cu} = 1eV [42] and E_{Cr} = 1.1 eV [43]. This may explain why these elements exhibit very close distributions of lifetime-vacancy cluster sizes.

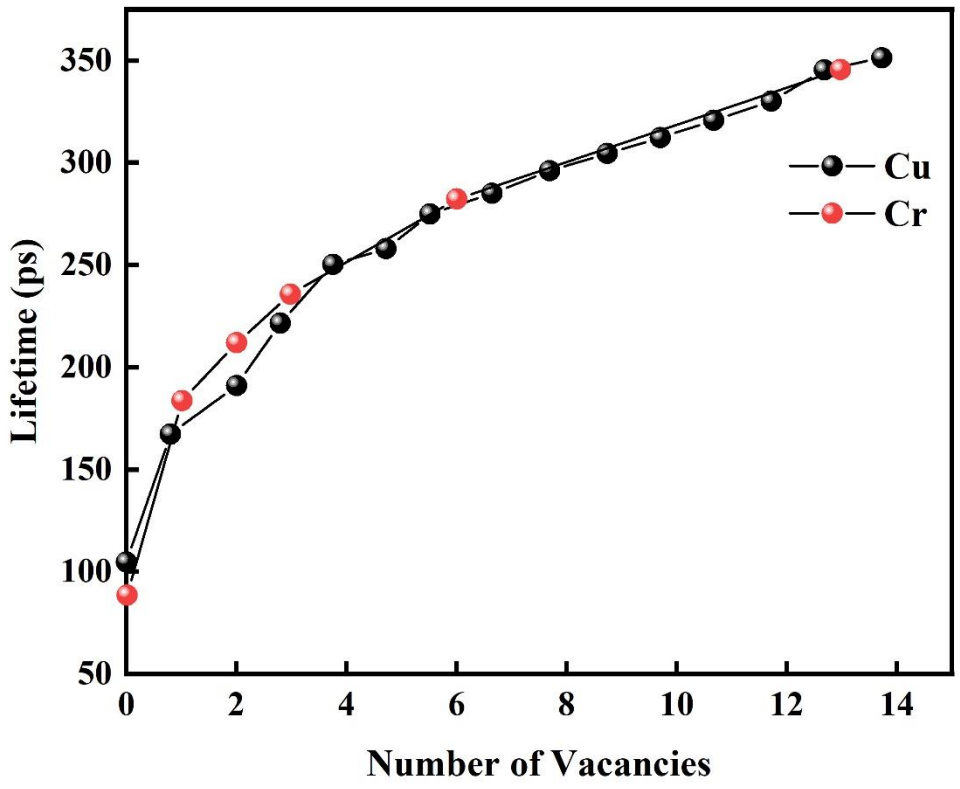

Figure 4: Calculated dependence of the positron lifetime on the size of vacancy clusters consisting of *N* vacancies in Cu [36] and Cr [33].

Table 2: Positron lifetime values for Cu and Cr tabulated in the literature. The subscript "c" stems from calculated values.

	Cu	Cr
Bulk [ps]	110 [32]c 120 [37] 115 [40]c	108 [33]c 120 [38]c 115 [40]c
Monovacancy [ps]	180 [34],[35]	188 [38]c 184 [30]
Dislocation [ps]	166 [34] 164 [34]	161 [30]

3.2 Microhardness evolution

The microhardness evolution with different measurement locations along the disc radius, r, of the Cu43%Cr alloy after HPT for (a) N = 5 turns and (b) N = 20 turns and with annealing are

shown in Figure 5. In practice, three measurement locations along the disc radius are r = 0 mm, r = R/2 and r = R, where R denotes the maximum radius of the discs of 5 mm. The as-received material without processing had an Hv value close to 112, which is indicated by dashed lines in the plots. HPT processing for 20 turns noted as N20-T25 caused a significant change at r = R/2 and R whereas it is not marked after 5 turns. In practice, the microhardness at the edge of the N20-T25 disk at r = R rises to 425 Hv, which is more than triple the as-received one. Such values are close to those reported by Guo et al. [1] which evidenced a fast increase in the hardness after torsion straining of $\varepsilon < 400$. In this high straining stage, the immiscible alloy hardens quickly due to the synergistic effect of grain refinement as well as the dissolution of Cu into the Cr matrix (forced intermixing). Specifically, a close inspection of the tabulated data reveals that Cu43%Cr alloy hardens more than those pure Cu after N = 5 turns [44, 45], and after 5 HPT turns of cu-based alloys such as Cu–0.1% Zr [46, 47], Cu–1.5% Si [48], Cu-2.5Ni-0.6Si [49]. There are some exceptions, such as the Cu–28% Ag alloy which exhibited a hardness of Hv≈350 after HPT 10 turns [50]. It should be noted that the present results as well as these reports showed lower hardness at the disc centers of $r \approx 0$ than the disc peripheries under the reported processing conditions.

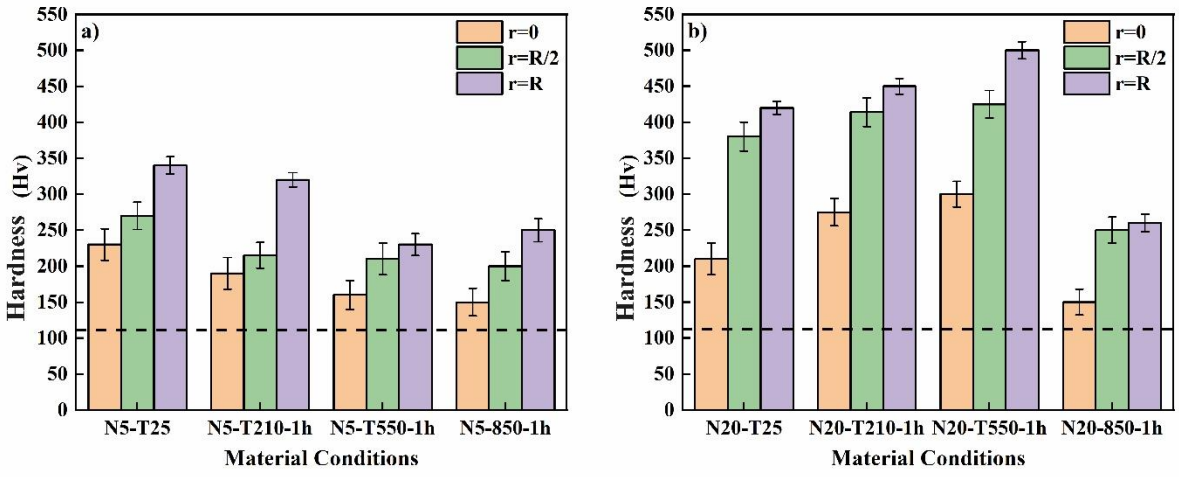

Figure 5: Evolution of the global microhardness of the Cu43%Cr alloy after HPT processing and annealing, a) 5 turns and, b) 20 turns.

The Cu43%Cr alloy after 5 HPT turns experienced softening after annealing at 210, 550 and 850°C for 1 hour owing to the dissolution of any supersaturated elements [18] with different levels of microstructural recovery, recrystallization followed by grain growth.

After processing up to 20 turns and annealing, the hardness evolution showed anneal hardening [51], where the result is unlike the one after HPT for 5 turns. In practice, hardness increases upon annealing at 210 and 550°C while a softening occurs after annealing at 850°C for 1 hour. A similar feature of anneal hardening was observed by Bachmaier et al. [18] in the Cu–Cr system after HPT for a high equivalent strain of 1590, while the report also demonstrated the consistent softening with annealing without strengthening when the system was deformed by HPT for an equivalent strain through 400.

While annealing hardening can appear in metals with different mechanisms, e.g. age hardening, Gubicza [51] reviewed the unique anneal hardening specifically for the SPD-processed nanostructured samples. The following three core reasons cause the extra hardening during annealing and heating in addition to the strengthening by grain refinement: (i) immigration of mobile dislocations within nanograins, and clustering into low energy configurations such as low-angle grain boundaries leading to dislocation annihilation, (ii) reduced emission of dislocation due to a relaxation of non-equilibrium grain boundaries, and (iii) hindering of the dislocation movement caused by clustering of excess vacancies introduced during SPD. While these three reasons may simultaneously influence the hardening of the alloy, the present results obtained by cPALS in Fig. 3 support the occurrence of anneal hardening by vacancy clusters in the disc with N=20 turns up to annealing temperatures of 550°C where dislocation annihilation was limited (see I1%) which occurred faster in the discs after N=5 turns. HPT processing and annealing at 210°C resulted in an agglomeration of up to about 10 vacancies.

The importance of vacancy clustering for anneal hardening may be demonstrated by the increase of I2% and the deagglomeration to about 4 vacancies after HPT followed by annealing above 550°C.

The anneal hardening effect has been the subject of controversial debate in the literature. Indeed, on the one hand, it has been assumed that the observed strengthening was ascribed to a reduction in the defect density and that it could occur at relatively low homologous temperatures and only in materials with grain sizes below a material specific threshold value [52]. On the other hand, the anneal hardening during heat treatment of HPT-processed pure Cu and Ni was ascribed to the agglomeration and annihilation of vacancies at homologous temperatures between T=0.25-0.3Tm [53].

Furthermore, the vacancy agglomeration and dislocation loops formation in the basal plane of an Mg-based alloy may act as strong obstacles to dislocation movement, and these phenomena may justify the observed anneal hardening in Mg-Zn-Ca alloys strengthened via high-pressure torsion (HPT) [54]. It is worth noting that a recent review has reported the state-of-art of this controversy [55]. The change of deformation induced grain boundaries through annealing of deformation induced vacancies has been quoted as the reason for anneal hardening but only for materials with a grain size below a certain threshold value. This value is far below those grain sizes found in the present study (d ~ 0.3 – 0.5 µm). As stated in the review [55], the influence of vacancy clusters on the anneal hardening is hindered upon decreasing the grain size. Plausibly this will play against the contribution of vacancy agglomerates to the anneal hardening as the principal cause.

Consistent with the explanation previously suggested [18], the enhanced extra anneal hardening may be assigned to restrictions in activating dislocation sources in the annealed material.

The hardness variation within the same processed and annealing condition for three different positions is unalike between N = 5 and N = 20 HPT turns. The hardness difference between

positions near the centre and at mid-radius and between mid-radius and edge has been systematically estimated for all conditions.

The hardness differences between r = 0 and r = R/2 varied weakly (13-17%) for the N=5 HPT processed and annealed at 210° and (31-33 %) between 550-850 °C. This confirms that the microstructure did not change drastically. The scatter is more important after processing at N = 20 turns (80 %). It seems to reduce to 41-60 % after annealing between 210-850 °C. This indicates that severe plastic deformation by HPT after N = 20 turns resulted in more inhomogeneity between the centre and the mid-radius.

For the sample after N = 5 HPT turns, the hardness difference between r = R/2 and r = R fluctuates and does not exhibit clear trends. While after N = 20 turns, the scatter varies moderately and ranges between 4 and 17 % owing to a certain saturation of the microstructure and hardness.

It is worth noting that such data are very scarce in the literature. Ibrahim et al. [56] have presented the results of the radial distribution of the Vickers hardness after HPT processing (N = 150 turns) in the as-prepared state and after successive annealing treatments in the range 200-1000 °C for 1 h. Across the radius, the hardness decreased monotonously in function of the annealing temperature. The authors stated that the systematic softening was ascribed to the precipitation hardening in the CuTa samples due to fine dispersed nano-sized Ta particles in the Cu grains.

Besides the grain refinement and dislocation storage mechanisms, Cizek et al. [41] have stated that an increase in the hardness may also probably be caused by an increase in the number of microvoids, which represent obstacles for the movement of dislocations. The hardening of the Cu43%Cr after HPT processing up to 5 and 20 turns may be ascribed to the grain refinement (down to 0.3-0 5 µm [22]) , dislocation density rise (from $4\ 10^{14}\ m^{-2}$ to $26\ 10^{14}\ m^{-2}$ [22]) and the increase of vacancy clusters (microvoids) from about n=4 to about n=10 vacancies.

Subsequently to annealing, the grain size remains unchanged whereas the dislocation density falls to that corresponding to the as received material [22]. The present study reveals that the number of vacancy clusters decreases from about n = 10-13 to about n = 4 vacancies. Therefore, only dislocation density and vacancy cluster decrease are responsible for the material softening. The hardness results could be correlated to the PAS results via the intensity of the existing defects. The as-received materials have a nominal hardness of 112 Hv and defects intensity of dislocations (I_1 = 40 %) and I_2 = 34 (clusters of vacancies, about n = 4). The HPT processing results in a global hardening up to 400 Hv and the dislocation intensity raises to 80% while that of clusters dropped down to 10% (about n = 8, 13). Annealing the HPT processed samples softened the alloy and I_1 decreased to 50% while I_2 slightly increased up to 30%. The ultimate softening is due, as discussed above, to recovery phenomena. Interestingly, HPT processing has shown a growth of the vacancy clusters from n = 3 to n = 13. After annealing, these defect clusters are no longer stable, which means the generated point defects annihilate and reduce their vacancy cluster size down to about n = 4. They should contribute to the overall softening.

Quite similar to the present results discrepancies of the microhardness values between the center and edge of the discs were already discussed in the literature.

A detailed microstructural observation through microhardness measurements in Cu-2.5Ni-0.6Si alloy processed by HPT [57] shows a gradual evolution with increasing numbers of revolutions with a saturation after 3 turns. Lower straining (N = 1/2 to N = 3 turns) fails to ensure global homogeneity and microhardness saturation. A 2D- graphic image was drawn showing the microhardness over a one-quarter zone of the surface of Al7075 alloy discs processed by HPT up to 5 turns [58].

This study revealed a soft (relatively to the edge) extended zone close to the center of the discs after ½ HPT turns. This soft zone is reduced upon increasing strain so that a more or less homogeneity is achieved with a notable hardening [58].

Processing by HPT generally involves the use of a thin disc that is subjected to high pressure and torsional straining. In practice, the equivalent von Mises strain, ε_{eq}, imposed on the disc in HPT is given by a relationship of the form [59]:

$$\varepsilon_{eq} = \frac{2\pi N r}{h\sqrt{3}} \qquad (3)$$

where h is the height (or thickness) of the disc. It follows from Eq. (3) that the strain varies across the disc from zero strain at the disc center where r = 0 to a maximum at the edge of the disc. Equation (3) predicts noteworthy inhomogeneities in the measured hardness values across the disc. However, many authors [60], stated that microstructural evolution occurs during processing and after large numbers of turns it was often possible to achieve a reasonable level of homogeneity. Theoretical analysis based on the application of strain gradient plasticity modeling [61] has also predicted the evolution of homogeneity.

Cizek et al. [28] have reviewed the results of Doppler Broadening (DB) of positron annihilation radiation and its correlation with microhardness distribution in many (Al, Ni, Cu), bcc (Fe, Nb, W) UFG metals. Their results indicated that dislocation density tends to saturate with strain. Moreover, the spatial distribution of vacancy clusters remains non-uniform even in samples subjected to a high number of HPT revolutions. The average size of vacancy clusters increases with radial distance from the center of the sample due to the increasing production rate of vacancies. Finally, as mentioned by Cizek et al. [28] H_V mapping highlights the grain refinement and dislocation density across the sample but not the spatial distribution of vacancies because the vacancy induced hardening is relatively faint and therefore, microhardness testing is insensitive against it. Therefore, a more suitable vacancy sensitive technique should be used in order to reveal the spatial distribution and homogeneity of these defects in the UFG materials.

Conclusions

The study of defect microstructure in a Cu43Cr alloy after HPT processing and annealing using two different positron annihilation spectroscopy (PAS) techniques, namely Doppler broadening

– variable energy PAS (DB-VEPAS) and conventional positron annihilation lifetime spectroscopy (cPALS) allows to draw the following conclusions:

The DB-VEPAS analysis of the near-surface defects reveals the existence of a nanosized layer of oxide whose thickness increases (43-103 nm) upon increasing the annealing temperature while the diffusion length was found constant around 20 nm. The type of defects is invariant. cPALS analysis of the bulk defects evidenced two major components for the as received and annealed at 925°C, HPT processed and annealed alloys.

For HPT processed and annealed samples the two components correspond to positrons trapped and annihilated at dislocations (lifetime~160 ps) in Cu and Cr and at clusters of vacancies with (about 13 and 10 vacancies).

After annealing the HPT-processed alloys, the first component and its intensity decrease with increasing annealing temperature which means that there is a partial annihilation of dislocations and recovery of the microstructure. The variation of the second component results from the variation in vacancy cluster size (from about 13 to about 4 vacancies) due to annealing.

A significant evolution in the microhardness values after processing by HPT up to 20 turns while a less pronounced one is depicted after N = 5 turns. The hardness evolution near the center, mid-radius and edge of the discs of the Cu43%Cr alloy after HPT processing and annealing at 210, 550 and 850°C for 1 hour is characterized by a softening of the material due to The results of the microhardness correlated well with the intensity of the point defects (dislocations and vacancy clusters).

Acknowledgement

The authors wish to thank Dr. Christophe Carrie from PLANSEE (Reutte, Austria) for supplying the Cu43Cr alloy. DB and IB are grateful to Prof. Ahmed Chafik Chami from Faculty of Physics (USTHB, Algiers) for the fruitful and improving discussions.

Declaration of interests

The authors declare that they have no known competing financial interests or personal relationships that could have appeared to influence the work reported in this paper.

References :

[1] J. Guo, J. M. Rosalie, R. Pippan, et Z. Zhang, « Revealing the Microstructural evolution in Cu-Cr nanocrystalline alloys during high pressure torsion », Materials Science and Engineering: A, vol. 695, p. 350-359, mai 2017, doi: 10.1016/j.msea.2017.04.034.

[2] S. Bera, S. Ghosh Chowdhury, W. Lojkowsky, et I. Manna, « Synthesis of CuCr and CuCrAg alloys with extended solid solubility with nano-Al2O3 dispersion by mechanical alloying and consolidation by high pressure sintering », Materials Science and Engineering: A, vol. 558, p. 298-308, déc. 2012, doi: 10.1016/j.msea.2012.08.004.

[3] S. Mula, J. Panigrahi, P. C. Kang, et C. C. Koch, « Effect of microwave sintering over vacuum and conventional sintering of Cu based nanocomposites », Journal of Alloys and Compounds, vol. 588, p. 710-715, mars 2014, doi: 10.1016/j.jallcom.2013.11.222.

[4] H. Kojima et al., « Conditioning mechanism of Cu-Cr electrode based on electrode surface state under impulse voltage application in vacuum », IEEE Trans. Dielect. Electr. Insul., vol. 18, n° 6, p. 2108-2114, déc. 2011, doi: 10.1109/TDEI.2011.6118651.

[5] S.-H. Chang, S.-H. Chen, K.-T. Huang, et C. Liang, « Improvement in sintering characteristics and electrical properties of Cr60Cu40 alloy targets by hot isostatic pressing treatment », Powder Metallurgy, vol. 56, n° 1, p. 77-82, févr. 2013, doi: 10.1179/1743290112Y.0000000038.

[6] L.-M. Peng, X.-M. Mao, K.-D. Xu, et W.-J. Ding, « Property and thermal stability of in situ composite Cu–Cr alloy contact cable », Journal of Materials Processing Technology, vol. 166, n° 2, p. 193-198, août 2005, doi: 10.1016/j.jmatprotec.2004.08.013.

[7] X. Sun, J. Jie, T. Wang, et T. Li, « Effect of two-step cryorolling and aging on mechanical and electrical properties of a Cu–Cr–Ni–Si alloy for lead frames applications », Materials Science and Engineering: A, vol. 809, p. 140521, mars 2021, doi: 10.1016/j.msea.2020.140521.

[8] Ph. Kiryukhantsev-Korneev et al., « Hard Wear-Resistant Ti-Si-C Coatings for Cu-Cr Electrical Contacts », Materials, vol. 16, n° 3, p. 936, janv. 2023, doi: 10.3390/ma16030936.

[9] R. K. Islamgaliev, K. M. Nesterov, J. Bourgon, Y. Champion, et R. Z. Valiev, « Nanostructured Cu-Cr alloy with high strength and electrical conductivity », Journal of Applied Physics, vol. 115, n° 19, p. 194301, mai 2014, doi: 10.1063/1.4874655.

[10] C. Watanabe, R. Monzen, et K. Tazaki, « Mechanical properties of Cu–Cr system alloys with and without Zr and Ag », J Mater Sci, vol. 43, n° 3, p. 813-819, févr. 2008, doi: 10.1007/s10853-007-2159-8.

[11] K. B. Gerasimov, S. V. Mytnichenko, S. V. Pavlov, V. A. Chernov, et S. G. Nikitenko, « Structural study of mechanically alloyed Cu30Cr70 by anomalous X-ray diffraction

and EXAFS-spectroscopy », Journal of Alloys and Compounds, vol. 252, nº 1-2, p. 179-183, mai 1997, doi: 10.1016/S0925-8388(96)02668-0.

[12] X. Sauvage, P. Jessner, F. Vurpillot, et R. Pippan, « Nanostructure and properties of a Cu–Cr composite processed by severe plastic deformation », Scripta Materialia, vol. 58, nº 12, p. 1125-1128, juin 2008, doi: 10.1016/j.scriptamat.2008.02.010.

[13] K. S. Kormout, R. Pippan, et A. Bachmaier, « Deformation-Induced Supersaturation in Immiscible Material Systems during High-Pressure Torsion », Adv Eng Mater, vol. 19, nº 4, p. 1600675, avr. 2017, doi: 10.1002/adem.201600675.

[14] C. Aguilar, V. de P. Martinez, J. M. Palacios, S. Ordoñez, et O. Pavez, « A thermodynamic approach to energy storage on mechanical alloying of the Cu–Cr system », Scripta Materialia, vol. 57, nº 3, p. 213-216, août 2007, doi: 10.1016/j.scriptamat.2007.04.006.

[15] C. Michaelsen, C. Gente, et R. Bormann, « Phase formation and thermodynamics of unstable Cu–Cr alloys », J. Mater. Res., vol. 12, nº 6, p. 1463-1467, juin 1997, doi: 10.1557/JMR.1997.0201.

[16] A. N. Patel et S. Diamond, « The effects of non-equilibrium processing in the development of copper alloys », Materials Science and Engineering, vol. 98, p. 329-334, févr. 1988, doi: 10.1016/0025-5416(88)90180-2.

[17] K. Zeng et M. Hämäläinen, « Thermodynamic analysis of stable and metastable equilibria in the Cu-Cr system », Calphad, vol. 19, nº 1, p. 93-104, mars 1995, doi: 10.1016/0364-5916(95)00010-C.

[18] A. Bachmaier, G. B. Rathmayr, M. Bartosik, D. Apel, Z. Zhang, et R. Pippan, « New insights on the formation of supersaturated solid solutions in the Cu–Cr system deformed by high-pressure torsion », Acta Materialia, vol. 69, p. 301-313, mai 2014, doi: 10.1016/j.actamat.2014.02.003.

[19] Q. Shao, J. Guo, J. Chen, et Z. Zhang, « Atomic-scale investigation on the structural evolution and deformation behaviors of Cu–Cr nanocrystalline alloys processed by high-pressure torsion », Journal of Alloys and Compounds, vol. 832, p. 154994, août 2020, doi: 10.1016/j.jallcom.2020.154994.

[20] A. R. Kilmametov, G. Vaughan, A. R. Yavari, A. LeMoulec, W. J. Botta, et R. Z. Valiev, « Microstructure evolution in copper under severe plastic deformation detected by in situ X-ray diffraction using monochromatic synchrotron light », Materials Science and Engineering: A, vol. 503, nº 1-2, p. 10-13, mars 2009, doi: 10.1016/j.msea.2008.11.023.

[21] W. Anwand, G. Brauer, M. Butterling, H. R. Kissener, et A. Wagner, « Design and Construction of a Slow Positron Beam for Solid and Surface Investigations », DDF, vol. 331, p. 25-40, sept. 2012, doi: 10.4028/www.scientific.net/DDF.331.25.

[22] I. Bibimoune et al., « An EBSD analysis of a commercial immiscible Cu43%Cr alloy after high-pressure torsion processing and annealing », Philosophical Magazine, p. 1-27, nov. 2023, doi: 10.1080/14786435.2023.2282023.

[23] E. Hirschmann et al., « A new system for real-time data acquisition and pulse parameterization for digital positron annihilation lifetime spectrometers with high repetition rates », Journal of Instrumentation, vol. 16, nº 08, p. P08001, août 2021, doi: 10.1088/1748-0221/16/08/P08001.

[24] J. V. Olsen, P. Kirkegaard, N. J. Pedersen, et M. Eldrup, « PALSfit: A new program for the evaluation of positron lifetime spectra », physica status solidi (c), vol. 4, n° 10, p. 4004-4006, sept. 2007, doi: 10.1002/pssc.200675868.

[25] F. Tuomisto et I. Makkonen, « Defect identification in semiconductors with positron annihilation: Experiment and theory », Rev. Mod. Phys., vol. 85, n° 4, p. 1583-1631, nov. 2013, doi: 10.1103/RevModPhys.85.1583.

[26] S. W. H. Eijt et al., « Positron depth profiling of the structural and electronic structure transformations of hydrogenated Mg-based thin films », Journal of Applied Physics, vol. 105, n° 4, p. 043514, févr. 2009, doi: 10.1063/1.3075762.

[27] K. V. Klinski-Wetzel, C. Kowanda, M. Heilmaier, et F. E. H. Mueller, « The influence of microstructural features on the electrical conductivity of solid phase sintered CuCr composites », Journal of Alloys and Compounds, vol. 631, p. 237-247, mai 2015, doi: 10.1016/j.jallcom.2014.12.249.

[28] J. Čížek et al., « The Development of Vacancies during Severe Plastic Deformation », Mater. Trans., vol. 60, n° 8, p. 1533-1542, août 2019, doi: 10.2320/matertrans.MF201937.

[29] A. Van Veen, H. Schut, M. Clement, J. M. M. De Nijs, A. Kruseman, et M. R. IJpma, « VEPFIT applied to depth profiling problems », Applied Surface Science, vol. 85, p. 216-224, janv. 1995, doi: 10.1016/0169-4332(94)00334-3.

[30] R. Auguste et al., « A multimodal approach to revisiting oxidation defects in Cr2O3 », npj Mater Degrad, vol. 6, n° 1, p. 61, juill. 2022, doi: 10.1038/s41529-022-00269-7.

[31] J. Čížek et al., « Investigation of spatial distribution of defects in ultra-fine grained copper », Applied Surface Science, vol. 194, n° 1-4, p. 140-144, juin 2002, doi: 10.1016/S0169-4332(02)00114-9.

[32] M. Hatakeyama et al., « 3D-AP and positron annihilation study of precipitation behavior in Cu–Cr–Zr alloy », Journal of Nuclear Materials, vol. 386-388, p. 852-855, avr. 2009, doi: 10.1016/j.jnucmat.2008.12.266.

[33] T. Troev, A. Markovski, S. Peneva, et T. Yoshiie, « Positron lifetime calculations of defects in chromium containing hydrogen or helium », Journal of Nuclear Materials, vol. 359, n° 1-2, p. 93-101, déc. 2006, doi: 10.1016/j.jnucmat.2006.07.020.

[34] J. Čížek et al., « Thermal stability of ultrafine grained copper », Phys. Rev. B, vol. 65, n° 9, p. 094106, févr. 2002, doi: 10.1103/PhysRevB.65.094106.

[35] H. E. Schaefer, W. Stuck, F. Banhart, et W. Bauer, « Thermal Vacancies in the Noble Metals Cu, Ag, Au and in Pt Studied by Positron Lifetime Spectroscopy », MSF, vol. 15-18, p. 117-124, janv. 1987, doi: 10.4028/www.scientific.net/MSF.15-18.117.

[36] J. Čížek, O. Melikhova, Z. Barnovská, I. Procházka, et R. K. Islamgaliev, « Vacancy clusters in ultra fine grained metals prepared by severe plastic deformation », J. Phys.: Conf. Ser., vol. 443, p. 012008, juin 2013, doi: 10.1088/1742-6596/443/1/012008.

[37] P. Horodek, J. Dryzek, et V. A. Skuratov, « Positron annihilation study of defects in copper irradiated with swift Xe 26+ ions », Vacuum, vol. 138, p. 15-21, avr. 2017, doi: 10.1016/j.vacuum.2017.01.013.

[38] J. M. C. Robles, E. Ogando, et F. Plazaola, « Positron lifetime calculation for the elements of the periodic table », J. Phys.: Condens. Matter, vol. 19, n° 17, p. 176222, avr. 2007, doi: 10.1088/0953-8984/19/17/176222.

[39] H. Ohkubo, Z. Tang, Y. Nagai, M. Hasegawa, T. Tawara, et M. Kiritani, « Positron annihilation study of vacancy-type defects in high-speed deformed Ni, Cu and Fe », Materials Science and Engineering: A, vol. 350, nº 1-2, p. 95-101, juin 2003, doi: 10.1016/S0921-5093(02)00705-0.

[40] J. Kuriplach et B. Barbiellini, « Gradient correction scheme for bulk and defect positron states in materials: New developments », J. Phys.: Conf. Ser., vol. 505, p. 012040, avr. 2014, doi: 10.1088/1742-6596/505/1/012040.

[41] J. Cizek et al., « Ultra Fine Grained Copper Prepared by High Pressure Torsion: Spatial Distribution of Defects from Positron Annihilation Spectroscopy », in Nanomaterials by Severe Plastic Deformation, M. Zehetbauer et R. Z. Valiev, Éd., Weinheim, FRG: Wiley-VCH Verlag GmbH & Co. KGaA, 2005, p. 407-412. doi: 10.1002/3527602461.ch7b.

[42] Yu. M. Plishkin et I. E. Podchinenov, « Vacancy migration energy calculation in an F.C.C. copper lattice by computer simulation », Phys. Stat. Sol. (a), vol. 38, nº 1, p. 51-55, nov. 1976, doi: 10.1002/pssa.2210380104.

[43] P.-W. Ma et S. L. Dudarev, « Effect of stress on vacancy formation and migration in body-centered-cubic metals », Phys. Rev. Materials, vol. 3, nº 6, p. 063601, juin 2019, doi: 10.1103/PhysRevMaterials.3.063601.

[44] Z. Horita et T. G. Langdon, « Microstructures and microhardness of an aluminum alloy and pure copper after processing by high-pressure torsion », Materials Science and Engineering: A, vol. 410-411, p. 422-425, nov. 2005, doi: 10.1016/j.msea.2005.08.133.

[45] A. P. Zhilyaev, A. A. Gimazov, G. I. Raab, et T. G. Langdon, « Using high-pressure torsion for the cold-consolidation of copper chips produced by machining », Materials Science and Engineering: A, vol. 486, nº 1-2, p. 123-126, juill. 2008, doi: 10.1016/j.msea.2007.08.070.

[46] J. Wongsa-Ngam, M. Kawasaki, Y. Zhao, et T. G. Langdon, « Microstructural evolution and mechanical properties of a Cu–Zr alloy processed by high-pressure torsion », Materials Science and Engineering: A, vol. 528, nº 25-26, p. 7715-7722, sept. 2011, doi: 10.1016/j.msea.2011.06.056.

[47] J. Wongsa-Ngam, M. Kawasaki, et T. G. Langdon, « Achieving homogeneity in a Cu–Zr alloy processed by high-pressure torsion », J Mater Sci, vol. 47, nº 22, p. 7782-7788, nov. 2012, doi: 10.1007/s10853-012-6587-8.

[48] H. Jiang, Y. T. Zhu, D. P. Butt, I. V. Alexandrov, et T. C. Lowe, « Microstructural evolution, microhardness and thermal stability of HPT-processed Cu », Materials Science and Engineering: A, vol. 290, nº 1-2, p. 128-138, oct. 2000, doi: 10.1016/S0921-5093(00)00919-9.

[49] H. Matsunaga, Z. Horita, K. Imamura, T. Kiss, et X. Sauvage, « Aging Behavior of Cu-Ni-Si Alloy Processed by High-Pressure Torsion », MSF, vol. 667-669, p. 307-312, déc. 2010, doi: 10.4028/www.scientific.net/MSF.667-669.307.

[50] Y. Z. Tian, S. D. Wu, Z. F. Zhang, R. B. Figueiredo, N. Gao, et T. G. Langdon, « Strain hardening behavior of a two-phase Cu–Ag alloy processed by high-pressure torsion », Scripta Materialia, vol. 65, nº 6, p. 477-480, sept. 2011, doi: 10.1016/j.scriptamat.2011.06.004.

[51] J. Gubicza, « Annealing-Induced Hardening in Ultrafine-Grained and Nanocrystalline Materials », Adv Eng Mater, vol. 22, nº 1, p. 1900507, janv. 2020, doi: 10.1002/adem.201900507.

[52] O. Renk, A. Hohenwarter, B. Schuh, J. H. Li, et R. Pippan, « Hardening by annealing: insights from different alloys », IOP Conf. Ser.: Mater. Sci. Eng., vol. 89, p. 012043, août 2015, doi: 10.1088/1757-899X/89/1/012043.

[53] P. Cengeri, M. B. Kerber, E. Schafler, M. J. Zehetbauer, et D. Setman, « Strengthening during heat treatment of HPT processed copper and nickel », Materials Science and Engineering: A, vol. 742, p. 124-131, janv. 2019, doi: 10.1016/j.msea.2018.11.010.

[54] J. Horky et al., « Exceptional Strengthening of Biodegradable Mg-Zn-Ca Alloys through High Pressure Torsion and Subsequent Heat Treatment », Materials, vol. 12, nº 15, p. 2460, août 2019, doi: 10.3390/ma12152460.

[55] O. Renk et R. Pippan, « Anneal Hardening in Single Phase Nanostructured Metals », Mater. Trans., vol. 64, nº 7, p. 1464-1473, juill. 2023, doi: 10.2320/matertrans.MT-MF2022029.

[56] N. Ibrahim, M. Peterlechner, F. Emeis, M. Wegner, S. V. Divinski, et G. Wilde, « Mechanical alloying via high-pressure torsion of the immiscible Cu50Ta50 system », Materials Science and Engineering: A, vol. 685, p. 19-30, févr. 2017, doi: 10.1016/j.msea.2016.12.106.

[57] A. Y. Khereddine, F. H. Larbi, M. Kawasaki, T. Baudin, D. Bradai, et T. G. Langdon, « An examination of microstructural evolution in a Cu–Ni–Si alloy processed by HPT and ECAP », Materials Science and Engineering: A, vol. 576, p. 149-155, août 2013, doi: 10.1016/j.msea.2013.04.004.

[58] S. Sabbaghianrad et T. G. Langdon, « A critical evaluation of the processing of an aluminum 7075 alloy using a combination of ECAP and HPT », Materials Science and Engineering: A, vol. 596, p. 52-58, févr. 2014, doi: 10.1016/j.msea.2013.12.034.

[59] R. Z. Valiev, Yu. V. Ivanisenko, E. F. Rauch, et B. Baudelet, « Structure and deformaton behaviour of Armco iron subjected to severe plastic deformation », Acta Materialia, vol. 44, nº 12, p. 4705-4712, déc. 1996, doi: 10.1016/S1359-6454(96)00156-5.

[60] T. G. Langdon, « Strengthening and weakening in the processing of ultrafine-grained metals », km, vol. 53, nº 04, p. 213-219, 2016, doi: 10.4149/km_2015_4_213.

[61] Y. Estrin, A. Molotnikov, C. Davies, et R. Lapovok, « Strain gradient plasticity modelling of high-pressure torsion », Journal of the Mechanics and Physics of Solids, vol. 56, nº 4, p. 1186-1202, avr. 2008, doi: 10.1016/j.jmps.2007.10.004.